8.06 Turbulence and Small-Scale Dynamics in the Core

D. E. Loper, Florida State University, Tallahassee, FL, USA

8.06.1 Introduction

8.06.1.1 What Is Turbulence?

Turbulence is fluid motion that is chaotic in time and space. It is characterized by vortices and eddies on many scales. Fluid motions that are not turbulent are said to be laminar. It is difficult to define turbulence more precisely, as it takes many forms depending on circumstances. The classic definition of turbulence, arising in engineering and applied to flow in or around smooth bodies, is that instability of laminar motion which occurs when the Reynolds number exceeds approximately 2300. However, it is not unreasonable to characterize flow in Earth's mantle, for example, as turbulent, even though it occurs at a Reynolds number of order 10^{-20}. It is clear from this example that the Reynolds number is not always the best measure of the occurrence of turbulence. As explained below, it is not an appropriate measure for Earth's core; more appropriate measures of turbulence in Earth's core are the Lorentz and magnetic Reynolds numbers, quantifying the effects of rotation and the magnetic field.

8.06.1.2 Why Does Turbulence Occur?

One reason why turbulence occurs can be understood with reference to the momentum equation for an incompressible fluid:

$$\partial \mathbf{u}/\partial t + (\mathbf{u}\cdot\nabla)\mathbf{u} = -\nabla\Pi + \mathbf{F} \qquad [1]$$

where $\mathbf{u}$ is the fluid velocity, Π is the dynamic pressure, and $\mathbf{F}$ represents the forces per unit mass acting on the fluid. In classic Newtonian fluid dynamics, only the viscous force due to molecular viscosity contributes to $\mathbf{F}$:

$$\mathbf{F} = \mathbf{F}_{vm} = \nu\nabla^2\mathbf{u} \qquad [2]$$

where ν is the kinematic viscosity. The ratio of inertial to viscous forces is quantified by the Reynolds number

$$R_e = UL/\nu \qquad [3]$$

where U is a typical speed of fluid motion and L is a typical lengthscale. (If the flow structure of interest is characterized by several lengths, L is normally the smallest of these.) When the viscous force is small in comparison with inertial effects, the Reynolds number is large. Setting $\mathbf{F} = \mathbf{0}$ and assuming the flow to be steady, the momentum equation [1] simplifies to

$$(\mathbf{u}\cdot\nabla)\mathbf{u} = -\nabla\Pi \qquad [4]$$

This equation describes a special balance; the inertial term on the left-hand side is a full vector, with three scalar degrees of freedom, whereas the pressure term on the right is a gradient, having only one. If the balance described by [4] prevails, a large-scale steady laminar flow is possible. However, when this balance is perturbed by a velocity field of arbitrary structure, the inertial force can no longer be balanced by the pressure gradient. With $\mathbf{F}$ negligibly small, a steady force balance is not possible; the unsteady term in [1] must make up the difference. But this implies that the flow becomes unsteady, that is, unstable, leading to turbulence. The time-derivative term generates smaller scales of motion, and eventually scales are produced having $R_e = O(1)$, and $\mathbf{F}_{vm}$ restores the balance. In this example, the cascade of energy to smaller scales is driven by the nonlinear inertia term.

Classic homogeneous isotropic turbulence is described by equation [1] with $\mathbf{F}$ given by [2], together with the equation of conservation of mass:

$$\nabla\cdot\mathbf{u} = 0 \qquad [5]$$

Its behavior is characterized by a single parameter, the Reynolds number, given by [3]. This problem has been the subject of countless studies, and much of our intuition regarding turbulence is based on this problem. This is somewhat unfortunate in the present context, as turbulence in Earth's core bears little resemblance to classic homogeneous turbulence, and it is doubtful that fundamental concepts of homogeneity (independence of position), isotropy (independence of direction), and an inertial range (in which kinetic energy cascades, without dissipative loss, to progressively smaller spatial scales) apply to core turbulence. As explained in the following subsection, the forces affecting flow in the core are such that core motions and turbulence are both nonhomogeneous and anisotropic. In particular, whereas there are no preferred directions in isotropic turbulence, at least three are relevant to the dynamics of Earth's core. The existence of an inertial range relies on the dominant force balance in the momentum equation involving only conservative forces. As we shall see, this is not the case in Earth's core; the Lorentz force is dominant and dissipative.

8.06.1.3 Forces and Fluxes Affecting Core Turbulence

Turbulent motions take differing forms and have differing mathematical representations depending on the forces contributing to $\mathbf{F}$. Those relevant to Earth's fluid outer core include the Coriolis force, the Lorentz force, and buoyancy forces, due both to the ambient (background) stratification and to local density differences between plumes and their surroundings. (In this chapter, 'plume' means a small-scale parcel of buoyant material.)

Additionally the form of turbulence depends on the nature of the forcing for fluid motion. In general, motions are driven by movement of boundaries (forced convection) or by internal density differences (natural convection), with the former common in engineering and the latter in geophysics and astrophysics. This distinction is not sharp; in some circumstances, natural convection leads to large-scale flows (e.g., the Jet Stream in the atmosphere and the Gulf Stream in the ocean) which can be unstable and lead to turbulent motions that are similar to those driven by forced convection.

Motions in Earth's fluid outer core are due ultimately to radioactive heating and secular cooling. More specifically, motions are driven by sources of buoyancy at the inner core boundary (ICB) and core–mantle boundary (CMB); in the absence of these forcings, conduction of heat would cause the core fluid to evolve to a thermally stably stratified state. The sources at the ICB include buoyant material segregated into the outer core by the progressive solidification and growth of the inner core,

latent heat released by that solidification process, and heat sources (secular cooling, Ohmic heating, and possibly radioactivity) arising within the inner core. The sources at the CMB are much less certain. It is not known with any certainty whether or how much material is being transferred between the core and mantle. Such transfers will be ignored in what follows. Thermal buoyancy capable of driving convection is generated at the CMB only if the rate of transfer of heat from core to mantle exceeds the rate that heat is conducted down the adiabat in the outer core.

8.06.1.4   Features of Core Turbulence

While relatively few definitive statements can be made about core turbulence, there are two that appear to be undisputable:

- Turbulence in the core is anisotropic.
- There is no inertial range, in which transfers of kinetic energy between scales occurs without loss.

Anisotropy of fluid motions is due to the combined action of the Coriolis and Lorentz forces. Together, they act to inhibit fluid motions perpendicular to the plane defined by $\mathbf{\Omega}$ and $\mathbf{B}$, resulting in so-called pancake-shaped flow structures, elongated in that plane. Since the Lorentz force is dominant, it is an important factor in the transfer of kinetic energy between spatial scales of motion; since that force is dissipative, the transfer involves loss of kinetic energy (Moffatt, 1967, 1978; Davidson, 2000; see Section 8.06.4). While core turbulence has some similarities to geostrophic flows (which are strongly affected by the conservative Coriolis force; e.g., see Charney, 1971; Rhines, 1979; Pedlosky, 1987; Cambon et al., 1997; Cambon, 2001), the absence of an inertial range in core turbulence makes the two types of flows quite distinct.

8.06.1.5   Dynamic Regions in the Outer Core

The entire outer core is close to a well-mixed state, with composition and specific entropy nearly constant, independent of position (these variables change slowly with time). The small, spatially dependent deviations from this state are dynamically important and are the main focus of studies of core structure and dynamics, including the geodynamo problem. As a result of these deviations, there may exist as many as three dynamic regions in the outer core: a plume
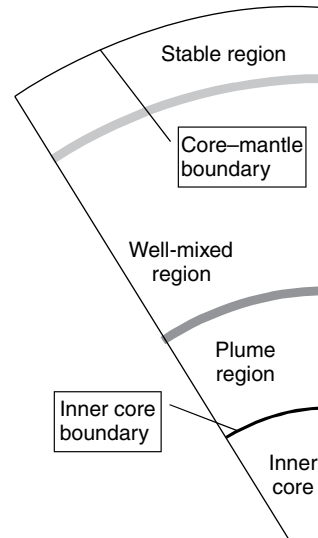

Figure 1   A cut-away view of the core, showing a plume region at the bottom of the outer core, a well-mixed region in the interior, and a stable region at the top. The radial extent of these regions is uncertain. The stable region may be well mixed by penetrative convective motions.

region at the bottom, a 'well-mixed' region in the middle, and a stable region at the top, as illustrated in **Figure 1**.

8.06.1.5.1   The plume region

The buoyancy released at the ICB due to solidification of the inner core creates very vigorous convection in the outer core (see [26] and discussion following). High-Rayleigh-number convective motions that are driven by a source of buoyancy at a boundary invariably consist of narrow rapid flows away from the boundary and slow, broad flows toward that boundary. The narrow, rapid motions upward from the ICB are likely to be small-scale plumes (i.e., elongated and flattened pancake-shaped structures). It follows that, near the bottom of the outer core, the area fraction, f, occupied by upwelling fluid is likely to be quite small; see **Figure 2**.

The plume region is characterized by the number, n, of plumes touching a given spherical surface located a distance r from Earth's center and the fraction, f, of area on that surface which they occupy. Both f and n are likely to be functions of r. The evolution of f and n with height above the ICB depends on the tendencies of plumes to entrain material, to merge, or to break up. Constraints on these variations are quantified in Section 8.06.5.2.
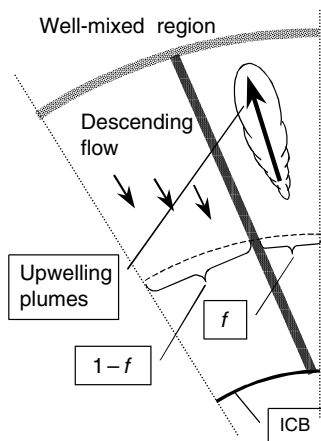
Figure 2 A cartoon of the plume region at the bottom of the outer core, showing upwelling plumes and descending flow occupying area fractions on spherical surfaces of magnitude f and $1 - f$, respectively, separated by the dark hatched line. The magnitude of f increases with radial distance from the center of the Earth and the top of the plume region is characterized by f being about 1/2. The upwelling and descending parts are shown separately for clarity; in reality, these are intermingled.

Close to the ICB, f is almost certainly very small (reflecting the general property of vigorous convection described previously). Where $f \ll 1$, it is reasonable to model plumes in isolation or to consider only two-plume interactions. The structure and scaling of the plume region are quantified in Sections 8.06.4 and 8.06.5.

8.06.1.5.2   The well-mixed interior region

It is likely that in the bulk of the outer core convective motions are turbulent, with buoyant and dense plumes of fluid ascending and descending, all the while interacting vigorously. The motions are strongly affected by Coriolis and Lorentz forces and, as in the plume region, very likely are pancake-shaped (Braginsky and Meytlis, 1990); see Section 8.06.4. Nearly all parametrizations of core turbulence are focused on this region. Current approaches to parametrization are summarized in Section 8.06.7.

8.06.1.5.3   A stable region beneath the CMB?

It is possible that fluxes of heat or composition tend to make the region at the top of the outer core dynamically stable. If the flux of heat to the mantle is less than that conducted down the adiabat, the excess heat will tend to produce a stabilizing thermal gradient near the top of the outer core. Similarly an upward flux of light material, either due to pressure diffusion or the upwelling of compositionally buoyant plumes, may tend to create a stabilizing compositional gradient near the top of the outer core (Braginsky, 1999).

Even if the fluxes of heat and composition tend to produce stabilizing gradients at the top of the outer core, penetrative convective motions originating in the convectively unstable interior of the outer core may maintain a well-mixed state all the way to the CMB. Further, it is likely that the strength of the heat transferred to the mantle varies with location on the CMB, so that the stable region is confined to 'patches' at the top of the outer core where the heat flow from core to mantle is relatively small.

If a stable layer does exist, it is incapable of significant dynamo action, which requires vigorous radial motion. Consequently it has received relatively little attention and will not be considered further in this chapter.

8.06.2   Governing Equations

It is likely that convective motions in the outer core are driven by density differences of both thermal and compositional origin. As will be seen below, these density differences are very small perturbations on a reference state that is hydrostatic, adiabatic (having uniform specific entropy), and well mixed (having uniform composition).

Following Braginsky and Roberts (1995), thermodynamic variables in the outer core will be expressed as the sum of a reference-state portion, denoted by subscript 'a', plus a small convective portion, denoted by a subscript 'c'. (The velocity, having no reference-state portion, is written without subscript.) The myriad of variables introduced in this chapter are summarized in **Table 1**.

8.06.2.1   Reference State

The reference state satisfies the equations of state $\rho_a C_p \nabla T_a = \alpha T_a \nabla p_a$ and $K_S \nabla \rho_a = \rho_a \nabla p_a$ plus the hydrostatic and well-mixed equations $\nabla p_a = -\rho_a \mathbf{g}_a$ and $\nabla c_a = \mathbf{0}$, where T is temperature, p pressure, ρ density, α coefficient of thermal expansion, C_p specific heat at constant pressure, K_S adiabatic incompressibility, and c mass fraction of light constituent (called the composition in the following). Note that the Gruneisen parameter, $\gamma = \alpha K_S / \rho_a C_p$, is dimensionless and of unit order in the outer core.

Table 1   Notation and definition of symbols

Symbol	Name	Dimensions and magnitude
a, b, c	Components of the dimensionless perturbation magnetic field (Section 8.06.4 only); see [32]	
A_p	Dimensionless horizontal area of a plume; see [45]	
B	Magnetic field vector	Wb m^{-2}
$\mathbf{B}_0$	Large-scale magnetic field vector	Wb m^{-2}
B_0	Typical magnitude of the magnetic field	$\approx 3 \times 10^{-3} \text{ Wb m}^{-2}$
c	Mass fraction of light constituent	
$\dot{c}_a$	Rate of increase of light material in the outer core; see [11] and [77]	$\sim 9 \times 10^{-20} \text{ s}^{-1}$
C	Co-density	
$\widehat{C}$	Scaled co-density; see [34]	
$\dot{C}$	Time rate of change of co-density; see [72]	$\sim 5 \times 10^{-20} \text{ s}^{-1}$
C_0	Typical magnitude of co-density	See [60]
C_p	Specific heat at constant pressure	$\text{J kg}^{-1} \text{ K}^{-1}$
C_{pe}	Effective specific heat of outer core	$\approx 1700 \text{ J kg}^{-1} \text{ K}^{-1}$
$\bar{C}_p$	Mass averaged specific heat	$\approx 800 \text{ J kg}^{-1} \text{ K}^{-1}$
C_{gr}	Effective specific heat for gravitational energy; see [85]	$\approx 300 \text{ J kg}^{-1} \text{ K}^{-1}$
C_{lh}	Effective specific heat for latent heat; see [86]	$\approx 600 \text{ J kg}^{-1} \text{ K}^{-1}$
D	Material diffusivity	$\approx 7 \times 10^{-9} \text{ m}^2 \text{ s}^{-1}$
f	Fraction of area occupied by plumes	See [59]
F_S	Divergence of flux of specific entropy	W K^{-1}
F_C	Divergence of flux of composition	$\sim 3 \times 10^{-21} \text{ s}^{-1}$
F	Body force	N
$\mathbf{F}_\nu$	Body force due to viscosity	N
$\mathbf{F}_{\nu m}$	Body force due to molecular viscosity	N
$\mathbf{g}_a$	Gravity vector in the reference state	m s^{-2}
$\bar{g}$	Mass-average magnitude of gravity in the outer core	$= 8.56 \text{ m s}^{-2}$
g	Acceleration of gravity	m s^{-2}
G	Smoothing operator; see [76]	
h	Depth or distance	m
J	Buoyancy flux	$\text{m}^4 \text{ s}^{-3}$
$\mathbf{J}_{icb}$	Buoyancy flux at the base of the outer core	$\sim \{15 \rightarrow 125\} \text{ m}^4 \text{ s}^{-3}$
$\mathbf{J}_c$	Buoyancy flux due to composition	$\text{m}^4 \text{ s}^{-3}$
k	Thermal conductivity	$\approx 28 \text{ W m}^{-1} \text{ K}^{-1}$
K_S	Adiabatic incompressibility	N m^{-2}
L	Typical length scale; also see [30]	See [62]
L_H	Latent heat of fusion	J kg^{-1}
m	Mass	kg
M	Mass within radius r	kg
M_c	Mass of core	$= 1.94 \times 10^{24} \text{ kg}$
M_{ic}	Mass of inner core	$= 9.84 \times 10^{22} \text{ kg}$
M_{oc}	Mass of outer core	$= 1.84 \times 10^{24} \text{ kg}$
$\dot{M}$	Convective mass flux	kg s^{-1}
$\dot{M}_{ic}$	Rate of growth of inner-core mass	$\sim 3.5 \times 10^6 \text{ kg s}^{-1}$
n	Number of plumes on a spherical surface	See [58]
n_B	Number of plumes threading a line of force	
N	Brunt Väisälä frequency	s^{-1}
p_a	Pressure in the reference state	N m^{-2}
P	Scaled dynamic pressure; see [33]	W
P_c	Power due to compositional convection	W
q	Heat source per unit mass	W kg^{-1}
$q*$	Sum of internal heat sources; see [14]	W kg^{-1}
q_{od}	Specific rate of Ohmic decay	W kg^{-1}
q_{rd}	Specific rate of radioactive heating	W kg^{-1}
Q	Heat flux from core	W
Q_{cd}	Heat flux down the adiabat	W

(Continued)

Table 1   (Continued)

Symbol	Name	Dimensions and magnitude
Q_{ic}	Heat from inner core	W
Q_{lh}	Heat released by solidification	W
Q_{oh}	Ohmic heating	W
Q_{rd}	Heat released by radioactive decay	W
Q_{sc}	Heat flux due to secular cooling	W
r	Radial position	m
r	Radius	m
$\bar{r}$	Mass-averaged radius	2.76×10^6 m
s	Specific entropy	J kg^{-1} K^{-1}
$\dot{s}_a$	Time rate of change of specific entropy in the reference state; see [12]	W kg^{-1} K^{-1}
$\dot{s}_*$	Sources of specific entropy; see [13]	$\approx -3.7 \times 10^{-16}$ W kg^{-1} K^{-1}
t	Time	S
T	Temperature	K
$\bar{T}$	Mean temperature in outer core	≈ 4350 K
u	Fluid velocity	m s^{-1}
$\tilde{u}$	Smoothed velocity; see [76]	m s^{-1}
u, v, w	Plume velocity components; see [31]	m s^{-1}
U	Typical speed based on Coriolis force; see [18]	m s^{-1}
U_p	Typical speed of plumes; see [44]	See [61]
V_{ic}	Inner-core volume	$= 7.6 \times 10^{18}$ m^3
$\dot{V}_p$	Volume flux of plume material	$\sim 4 \times 10^9$ m^3 s^{-1}
$\dot{V}_{ic}$	Rate of growth of inner-core volume	m^3 s^{-1}
W	Speed of downwelling	m s^{-1}
x	Coordinate direction normal to the plane of **B** and Ω	m
x_{od}	Dimensionless Ohmic heating	Q_{od} 10^{-12} W^{-1}
x_{rd}	Dimensionless radioactive heating	Q_{rd} 10^{-12} W^{-1}
x_T	Dimensionless rate of cooling	$\approx [\mathrm{d}\bar{T}/\mathrm{d}t] 3 \times 10^{15}$ s K^{-1}
y	Third Cartesian coordinate	m
z	Coordinate aligned with Ω	m
α	Coefficient of thermal expansion	K^{-1}
α_s	Entropic expansion coefficient; $= \alpha T C_p$	$\approx 7 \times 10^{-5}$ K kg J^{-1}
β	Dimensionless distance along a field line; see [41]	
Γ	See [87]	
δ	Fractional jump in density due to change in composition across the inner-core boundary	≈ 0.05
ΔC_c	Jump in composition at the ICB; see [78]	
η_m	Magnetic diffusivity	≈ 2 m^2 s^{-1}
θ	Colatitude	radian
κ	Thermal diffusivity; $= k/\rho C_p$	m^2 s^{-1}
$\bar{\kappa}$	Mass-averaged thermal diffusivity	$\approx 3 \times 10^{-6}$ m^2 s^{-1}
λ	Angle between **B** and Ω; see [32]	radian
μ	Chemical potential	J kg^{-1}
$\hat{\mu}$	Chemical potential gradient	$\approx 4.4 \times 10^7$ J kg^{-1}
μ_m	Magnetic permeability	$= 4\pi \times 10^{-7}$ Wb^2 s^2 m kg^{-1}
ξ, η, ζ	Plume coordinates; see [35]	
Π	Dynamic pressure	N m^{-2}
ϕ	Local longitude	radian
ρ_a	Density of the reference state	kg m^{-3}
$\bar{\rho}$	Mass-averaged density of the reference state	$= 1.09 \times 10^4$ kg m^{-3}
$\bar{\rho}_{ic}$	Mass-averaged density of inner core	kg m^{-3}
τ	dimensionless time; see [35]	
τ_{ic}	Age of the inner core	s
τ_{oc}	Mean turnover time of the outer core	s
ν	Kinematic viscosity	$\approx 5 \times 10^{-7}$ m^2 s^{-1}
$\bar{\psi}$	Mean gravitational potential of outer core	$\approx 10^7$ J kg^{-1}
Ω	Rotation vector	s^{-1}

Table 1   (Continued)

Symbol	Name	Dimensions and magnitude
Ω	Rotation rate	$= 7.29 \times 10^{-5}\,\mathrm{s}^{-1}$
ICB	Inner-core boundary	
CMB	Core–mantle boundary	
Subscript 'a'	Adiabatic reference state	
Subscript 'c'	Convective perturbation	
E	Ekman number	[21]
R_e	Reynolds number	[3]
Λ	Lorentz number	[19]
R_o	Rossby number	[20]
R_m	Magnetic Reynolds number	[22]
R_a	Rayleigh number	[26]
S_{ch}	Schmidt number	[28]
P_r	Prandtl number	[29]

Magnitudes preceded by $=$ are reasonably well known, and typically have two significant digits; magnitudes preceded by $\approx$ are accurate to about one significant digit (or a bit less); magnitudes preceded by $\sim$ are rough approximations, with likely errors of 100%, and possibly more. A range of values is denoted by two numbers in curly brackets, separated by an arrow.
An additional dimensionless parameter is the Gruneisen parameter γ ($\alpha K_S/\rho_a C_P$).

Much of our information of core structure and composition comes from teleseismic measurements of the speed of sound, $\sqrt{K_S/\rho_a}$.

8.06.2.2   Convective Equations

The equations governing convective motions in the outer core are (*see* Chapter 8.05)

$$\partial \mathbf{u}/\partial t + (\mathbf{u}\cdot\nabla)\mathbf{u} + 2\mathbf{\Omega}\times\mathbf{u} = -\nabla\Pi + C\mathbf{g}_a + (\mathbf{B}\cdot\nabla)\mathbf{B}/\rho_a\mu_m + \mathbf{F}_v \quad [6]$$

$$\nabla\cdot(\rho_a\mathbf{u}) = 0 \quad [7]$$

$$\partial\mathbf{B}/\partial t + (\mathbf{u}\cdot\nabla)\mathbf{B} = (\mathbf{B}\cdot\nabla)\mathbf{u} - \nabla\times(\eta_m\nabla\times\mathbf{B}) \quad [8]$$

$$\nabla\cdot\mathbf{B} = 0 \quad [9]$$

$$C = -\alpha_s s_c - c_c \quad [10]$$

$$\partial c_c/\partial t + (\mathbf{u}\cdot\nabla)c_c = -F_c - \dot{c}_a \quad [11]$$

and

$$\partial s_c/\partial t + (\mathbf{u}\cdot\nabla)s_c = -F_s - \dot{s}_a + \dot{s}_* \quad [12]$$

where $\mathbf{u}$ is the fluid velocity, $\mathbf{\Omega}$ rotation vector, Π dynamic pressure, $\mathbf{g}_a$ reference-state gravity, C codensity, $\mathbf{B}$ magnetic field vector, $\mathbf{F}_v$ viscous force, μ_m magnetic permeability, η_m magnetic diffusivity, $\alpha_s = (\alpha T/C_p)_a$ entropic expansion coefficient, F_c divergence of flux of composition, $\dot{c}_a = dc_a/dt$ temporal rate of increase of light material in the outer core (due to the growth of the inner core), s specific

entropy (entropy per unit mass), F_s divergence of flux of specific entropy, $\dot{s}_a = ds_a/dt$ temporal rate of increase of specific entropy in the reference state, and

$$\dot{s}_* = q_*/T_a \quad [13]$$

represents the specific-entropy source due to heat sources (per unit mass) arising from radioactive decay, q_{rd}, Ohmic dissipation, q_{od}, and conduction of heat down the adiabat:

$$q_* = q_{rd} + q_{od} + (k/\rho_a)\nabla^2 T_a \quad [14]$$

with k being (molecular) thermal conductivity. Note that C is defined to be negative in buoyant plumes and that conduction of heat is a sink rather than a source of heat.

According to Roberts and Glatzmaier (2000), $\dot{c}_a \approx 9\times10^{-20}\,\mathrm{s}^{-1}$ and $\dot{s}_a \approx -3.7\times10^{-16}\,\mathrm{W\ kg}^{-1}\,\mathrm{K}^{-1}$. It is estimated in Appendix 1 that $\dot{s}_* = (2.6x_{rd} + 2.6x_{oh} - 7.5)\times10^{-16}\,\mathrm{W\ kg}^{-1}\,\mathrm{K}^{-1}$ where the rates of total heating $(Q = \int q dm)$ in the core due to radioactivity and Ohmic decay have been quantified by $x_{rd}\,10^{12}$ W and $x_{oh}\,10^{12}$ W, respectively.

By using the variables Π and C, several complications (involving the perturbations of density by pressure and gravity by density) have been sidestepped, although not ignored. Two advantages of using specific entropy rather than temperature in the density equation of state [10], are that the reference state has uniform specific entropy and that α_s is more nearly constant across the outer core than is the

thermal expansion coefficient, α [$(\alpha_s)_{icb}/(\alpha_s)_{cmb} = 0.78$ while $\alpha_{icb}/\alpha_{cmb} = 0.57$]. Using data from Stacey and Davis (2004), $\alpha_s \approx \{8.3, 6.5\} \times 10^{-5}$ K kgJ^{-1} at the {top, bottom} of the outer core.

In the case that only molecular processes act, $\mathbf{F}_v$ is given by [2],

$$F_c = -D[\nabla^2 c_c - \nabla \cdot (\rho_a \delta \mathbf{g}_a / \hat{\mu})] \qquad [15]$$

and

$$F_s = -k(\nabla^2 T_c)/\rho_a T_a \qquad [16]$$

where D is material diffusivity, $\delta = \partial \mu / \partial p$, $\hat{\mu} = \partial \mu / \partial c$, and μ is the chemical potential difference between the two constituents (with core material being modeled as a binary alloy of metal and nonmetal; see Loper and Roberts, 1981).

For molten iron alloys near the melting point, $D \approx 7 \times 10^{-9}$ m^2 s^{-1} (Chalmers, 1964; Poirier, 1988), while Loper and Roberts (1981) estimated that a plausible range for $\rho_a \delta$ is between 1 and 2.5 and that $\hat{\mu} \approx 4.4 \times 10^7$ J kg^{-1}. The magnitude of $\nabla^2 c_c$ is difficult to estimate, but it is likely not to exceed that of the second term in the square bracket on the right-hand side of [15]; that second term is dominated by the divergence of gravity. Altogether, $F_c \sim 3 \times 10^{-21}$ s^{-1}; this is negligibly small compared with $\dot{c}_a$, which has been estimated following [14]. The value of thermal conductivity in the outer core is somewhat uncertain. Stacey and Anderson (2001) estimated k to vary from 46 W m^{-1} K^{-1} at the CMB to 63 W m^{-1}K^{-1} just above the ICB. However, Stacey (personal communication, 2005) now prefers a value $k = 28$ W m^{-1} K^{-1}, with little variation with depth. The magnitude of $\nabla^2 T_c$ is also difficult to estimate, but for any reasonable estimates, $F_s \ll \dot{s}_a$.

To a good approximation α_s may be treated as a constant and F_s and F_c neglected. Now eqns [11] and [12] may be combined to yield an evolution equation for the co-density:

$$\partial C / \partial t + (\mathbf{u} \cdot \nabla) C = \alpha_s [\dot{s}_a - \dot{s}_*] + \dot{c}_a \qquad [17]$$

Taking $\alpha_s \approx 7 \times 10^{-5}$ K kgJ^{-1} and using previous estimates, the forcing term on the right-hand side of [17] is roughly $[12 - 1.8(x_{rd} + x_{oh})] \times 10^{-20}$ s^{-1}, where x_{rd} and x_{oh} were introduced in the discussion following [14].

The unparametrized form of the governing equations contain four molecular diffusivities, for momentum (ν), material (D), heat ($\kappa = k/\rho C_p$), and magnetic flux (η_m). While ν, D, and κ are small and thus appear to require parametrization, η_m is sufficiently large that parametrization is neither needed nor desirable.

8.06.3 Parameters and Scaling

In this section, the dimensionless parameters associated with the governing equations are presented and discussed, beginning in Section 8.06.3.1 with those arising in the momentum and magnetic-diffusion equations and concluding in Section 8.06.3.2 with those arising in the equations governing variation of composition and entropy.

8.06.3.1 Momentum and Magnetic Diffusion Equations

As noted in Section 8.06.1.4, the force balances in [6] are far different from those in the traditional form of the momentum equation, [1]. Whereas the dominant balance in [1] is between pressure and inertia with the viscous force typically being small, the dominant balance in [6] appears to involve Coriolis, Lorentz, pressure, and buoyancy forces, with inertia and viscosity being small, although possibly not negligible. By custom for rapidly rotating systems, the Coriolis force is used as the reference force, against which other forces are measured. Most of these comparisons are quantified by dimensionless parameters, considered below. The exceptions are the pressure and buoyancy forces, which, when compared with the Coriolis force, yield scales for the dynamic pressure and velocity. The pressure scale is not of interest, while the characteristic velocity, U, is normally given by

$$U = C_0 \bar{g}/2\Omega \qquad [18]$$

where $\Omega = \|\mathbf{\Omega}\| = 7.29 \times 10^{-5}$ s^{-1}, $\bar{g} = 8.56$ m s^{-2} is the mass-averaged magnitude of gravity in the outer core, and C_0 is a characteristic amplitude of C. (Here and below, an overbar denotes an average (of a variable but well-determined quantity) within the outer core, while a subscript '0' denotes a typical or characteristic value (of a quantity of somewhat uncertain magnitude). Also, an equal sign implies accuracy to roughly two significant digits, $\approx$ implies one significant digit (or a bit less), and $\sim$ implies likely errors of 100% or possibly more.) The velocity deduced from secular variation of the geomagnetic field (e.g., see figure 4.1 of Merrill et al., 1996), 0.38° yr$^{-1} \approx 7 \times 10^{-4}$ m s^{-1}, is produced by this scaling with $C_0 \approx 1.2 \times 10^{-8}$. It is shown in Section 8.06.4 that the rise speed of small-scale plumes can be greater than indicated by this velocity scale.

The Lorentz, inertial, and (molecular) viscous forces are quantified by the Elsasser, Rossby, and Ekman numbers, respectively:

$$\Lambda \equiv B_0^2 / \eta_m \mu_m \bar{\rho} 2\Omega \qquad [19]$$

$$R_o \equiv U / 2\Omega L \qquad [20]$$

and

$$E \equiv \nu / 2\Omega L^2 \qquad [21]$$

where B_0 is a typical magnitude of the magnetic field in the outer core and $\bar{\rho}$ is the mean density. In addition, an important measure of dynamo action is the magnetic Reynolds number:

$$R_m \equiv UL / \eta_m \qquad [22]$$

which quantifies the relative importance of induction and Ohmic dissipation. In the core $\eta_m \approx 2 \text{ m}^2 \text{ s}^{-1}$; this parameter is invariably treated as a constant.

For large-scale motions in the core, E is very small and Λ is roughly of unit order; $\Lambda = 1$ if $B_0 = \sqrt{\eta_m \mu_m \bar{\rho} 2\Omega} \approx 2 \times 10^{-3} \text{Wb m}^{-2}$. One physical interpretation of the Elsasser number is that it is the ratio of the Joule damping time, $\eta_m \mu_m \bar{\rho} / B_0^2$, to the period of rotation of Earth, $2\pi\Omega$. A unit-order Elsasser number implies a large Lorentz force, capable of damping flow structures (such as free vortices) on timescales of the order of 1 day. This illustrates one difficulty in maintaining the dynamo; if the magnetic field is to be maintained efficiently, it must be configured so that this damping is not strong. It is likely that the Elsasser number in the core is large; see Section 8.06.5.3.

While the magnitudes of dimensionless numbers are illustrative of the relevant force balances, they do not tell the entire story. In addition to magnitude, forces have three other relevant attributes: conservative/dissipative/source, linear/nonlinear, and degrees of freedom. Conservative forces, such as inertia, Coriolis, and pressure, redistribute kinetic energy but do not degrade it to heat. Dissipative forces, such as Lorentz (coupled with finite electrical resistivity) and viscous, act to dissipate kinetic energy. The buoyancy force acts as a source of kinetic energy, counterbalancing dissipation. A force is nonlinear if it involves a dependent variable more than once (e.g., inertia) or if it involves a dependent variable that is governed by a nonlinear equation (Lorentz, buoyancy). Degrees of freedom refers to the structure of a force vector. The forces that have three degrees of freedom and are fully three-dimensional (3-D) are inertia and (molecular) viscous. The Coriolis and Lorentz forces involve cross products which constrain them to have two degrees of freedom. Buoyancy acts in a fixed direction and so has one degree of freedom. Pressure, being the gradient of a scalar, also has only one degree of freedom. These properties are summarized in **Table 2**. Note that the viscous term is the only dissipative force having three degrees of freedom.

The limitation in the degrees of freedom of the Coriolis force results in the well-known Taylor–Proudman Theorem:

$$(\mathbf{\Omega} \cdot \nabla)\mathbf{u} = 0 \qquad [23]$$

This constraint is valid only at dominant order and only if the Coriolis force is much larger than the Lorentz force (i.e., if $\Lambda \ll 1$). By the same token, the limitation in the degrees of freedom of the Lorentz force (in the case that $\Lambda \gg 1$) impresses a similar structure on the velocity, but now with invariance in the direction of **B** rather than **Ω**. These two constraints, taken together, imply that fluid motions in Earth's outer core are pancake shaped (Braginsky and Meytlis, 1990; see Section 8.06.4).

As seen in **Table 2**, the momentum equation contains three nonlinear terms, representing the Lorentz, inertial, and buoyancy forces. The buoyancy force is nonlinear by virtue of the advection term in [17]; this is a primary source of nonlinearity in the mathematical problem governing convective motions in the outer core. The noninertial force is proportional to the Rossby number, defined by [20], and is small for flows which are sufficiently rapid or of sufficiently large scale that $R_o \ll 1$. It is shown in Section 8.06.4

Table 2   Summary of forces in outer-core dynamics

Force	Dominant or secondary	Conservative, dissipative, or source	Linear or nonlinear	Degrees of freedom
Coriolis	Dominant	Conservative	Linear	2
Lorentz	Dominant	Dissipative	Nonlinear	2
Pressure	Dominant	Conservative	Linear	1
Buoyancy	Dominant	Source	Nonlinear	1
Inertia	Secondary	Conservative	Nonlinear	3
Viscous	Secondary	Dissipative	Linear	3

that the inertial force is likely to be important in the dynamics of buoyant plumes and that the Lorentz force and accompanying magnetic diffusion equation may be linearized when considering buoyant plumes having small spatial and/or velocity scales such that $R_m \ll \Lambda$. In this limit, at dominant order in powers of R_m, equations [6] and [8] may be expressed as

$$\partial \mathbf{u}/\partial t + (\mathbf{u}\cdot\nabla)\mathbf{u} + 2\mathbf{\Omega} \times \mathbf{u} = -\nabla\Pi + C\mathbf{g}_a \\ + (\mathbf{B}_0\cdot\nabla)\mathbf{B}/\rho_a\mu_m + \mathbf{F}_v$$

[24]

and, with constant magnetic diffusivity,

$$(\mathbf{B}_0\cdot\nabla)\mathbf{u} = -\eta_m\nabla^2\mathbf{B}$$

[25]

where $\mathbf{B}_0$ is the large-scale magnetic field (to be treated as a constant). Buoyancy is a source of kinetic energy, through convective instability, only if the density distribution is favorable (e.g., heavy fluid above light). The tendency for, and strength of, convective instability is quantified by the Rayleigh number which, in the present case, is of the form

$$R_a = C_0\bar{g}b^3/\nu\bar{\kappa}$$

[26]

where $\bar{\kappa}$ is the appropriate (thermal or compositional) mass-averaged molecular diffusivity and b is a vertical distance. Instability occurs when denser fluid underlies lighter and R_a exceeds a critical value of roughly 1000. Typically R_a is very large in the outer core. For example, with $\bar{\kappa} \equiv k/\bar{\rho}\bar{C}_p$ and using $\bar{\rho} = 1.09 \times 10^4\,\text{kg m}^{-3}$ and $\bar{C}_p \approx 800\,\text{J kg}^{-1}\text{K}^{-1}$ (Stacey and Davis, 2004) plus $k = 28\,\text{W m}^{-1}\,\text{K}^{-1}$ (F. Stacey, personal communication, 2005), $\bar{\kappa} \approx 3 \times 10^{-6}\,\text{m}^2\,\text{s}^{-1}$. If the outer core ($b \approx 2.2 \times 10^6\,\text{m}$) has a heavy-over-light co-density contrast of, say, $C_0 \sim 10^{-9}$ with $\nu \approx 5 \times 10^{-7}\,\text{m}^2\,\text{s}^{-1}$, $\bar{g} \approx 8.56\,\text{m s}^{-2}$, then $R_a \sim 6 \times 10^{22}$, indicating extreme convective instability. With compositional diffusivity, the Rayleigh number is even larger. On the other hand, if the outer core had a light-over-heavy co-density contrast, the Brunt Väisälä frequency would be

$$N = \sqrt{\bar{g}C_0/b}$$

[27]

With previous estimates, $N \approx 6 \times 10^{-8}\,\text{s}^{-1} \approx 2\,\text{yr}^{-1}$. (Note that this estimate is for illustration only; it is not suggested here that the bulk of the outer core is stratified.)

8.06.3.2   Composition and Specific Entropy

Equations [11] and [12] with the diffusive forms of the flux divergences [15] and [16], when nondimensionalized, yield two dimensionless parameters

quantifying the relative strengths of advection and diffusion: the Schmidt and Peclet numbers are

$$S_{ch} = UL/D$$

[28]

and

$$P_r = UL/\bar{\kappa}$$

[29]

8.06.4   Scaling and Structure of Plumes

A dominant factor in structure of plumes in the outer core is the constraint imposed by rotation, quantified by [23] in the limit that buoyancy and Lorentz forces are negligibly small. If $\Lambda \geq O(1)$, this constraint is modified by the action of the Lorentz force in such a way that convective motions are facilitated. For example, the critical Rayleigh number for thermal convection in a rapidly rotating fluid decreases as the effect of the magnetic field increases (Chandrasekhar, 1961).

It is generally believed that the dynamo is in the strong-field regime (Roberts *et al.*, 2003; *see* Chapter 8.08), characterized by $\Lambda \gg 1$ in the bulk of the core. This suggests that, by adopting a suitable size and shape, the rise speed of plumes can exceed the magnitude predicted by [18]. On the other hand, the rise speed is limited by the condition that the Rossby number not exceed unity; only flows having a duration less than 1 day can have a large Rossby number. That is, the maximum characteristic rise speed is $2\Omega L$, where L is the thickness (i.e., smallest linear dimension) of the plume. In order that the characteristic speed of form [18] (with the mean value of gravity replaced by the local value) not exceed this maximum, the characteristic lengthscale must satisfy $L \geq C_0 g/4\Omega^2$. Detailed scaling of plume flow (presented below) reveals that L exceeds this lower bound in proportion to the Elsasser number; that is,

$$L = \frac{C_0 g \Lambda}{4\Omega^2}$$

[30]

Adopting this scaling, the velocity, magnetic field, and buoyancy may be expressed as (H. Shimizu, private communication, 2006)

$$\mathbf{u} = U[u\hat{\mathbf{x}} + \Lambda v\hat{\mathbf{y}} + \Lambda w\hat{\mathbf{z}}]$$

[31]

and

$$\mathbf{B} = B_0[\sin(\lambda)\hat{\mathbf{y}} + \cos(\lambda)\hat{\mathbf{z}}] + B_0 \frac{R_{\mathrm{m}}}{\Lambda}\left[\frac{1}{\Lambda}a\hat{\mathbf{x}} + b\hat{\mathbf{y}} + c\hat{\mathbf{z}}\right] \quad [32]$$

$$\Pi = \frac{C_0^2 g^2}{4\Omega^2}\Lambda^2 P \quad [33]$$

$$C = C_0 \widehat{C} \quad [34]$$

where x is a coordinate direction normal to the plane of $\mathbf{B}$ and $\mathbf{\Omega}$, z is aligned with the rotation axis (see **Figure 3**), C_0 is the magnitude of the buoyancy, and U is given by [18] with the mean magnitude of gravity replaced by the local value. The coordinates and time may be nondimensionalized as

$$\{x, y, z, t\} = \left\{L\xi,\ L\Lambda\eta,\ L\Lambda\zeta,\ \frac{1}{2\Omega}\Lambda\tau\right\} \quad [35]$$

It may be seen from [32] that the perturbation magnetic field is small provided that $R_{\mathrm{m}} \ll \Lambda$. Assuming this condition to be satisfied, the governing equations are, at dominant order in powers of Λ^{-1},

$$-v + \frac{\partial P}{\partial\xi} = 0 \quad [36]$$

$$\frac{Dv}{D\tau} + u + \frac{\partial P}{\partial\eta} + \sin(\theta)\sin(\phi)\widehat{C} = \sin(\lambda)\frac{\partial b}{\partial\beta} \quad [37]$$

$$\frac{Dw}{D\tau} + \frac{\partial P}{\partial\zeta} + \cos(\theta)\widehat{C} = \sin(\lambda)\frac{\partial c}{\partial\zeta} \quad [38]$$

$$\frac{\partial u}{\partial\xi} + \frac{\partial v}{\partial\eta} + \frac{\partial w}{\partial\zeta} = 0 \quad [39]$$

and

$$-\sin(\lambda)\frac{\partial}{\partial\beta}\{u,\ v,\ w\} = \frac{\partial^2}{\partial\xi^2}\{a,\ b,\ c\} \quad [40]$$
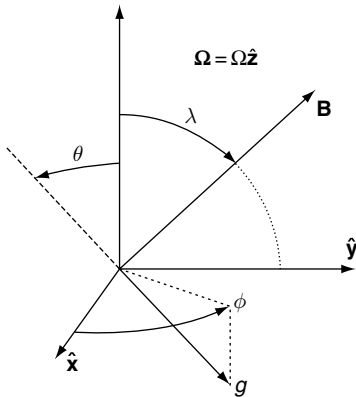

Figure 3 A depiction of the relative orientation of rotation, magnetic field and gravity vectors, and associated angles.

where θ is colatitude, ϕ is local longitude, and

$$\frac{\partial}{\partial\beta} = \frac{\partial}{\partial\eta} + \frac{\cos(\lambda)}{\sin(\lambda)}\frac{\partial}{\partial\zeta} \quad [41]$$

is a derivative in the direction of the large-scale magnetic field.

Equations [36]–[40], together with a suitably non-dimensionalized version of [17], constitute a set of eight equations for eight unknowns: a, b, c, u, v, w, P, and $\widehat{C}$. The forcing function for this set of homogeneous equations is in the initial or boundary condition for $\widehat{C}$. Energy is provided to the flow by the buoyancy terms $\widehat{C}$ in [37] and [38] and is dissipated by the Lorentz terms in the same equations.

Although the aspect ratio of plumes governed by this set of equations is the same as that proposed by Braginsky and Meytlis (1990), there are some differences between the two approaches. Whereas Braginsky and Meytlis conceived of transient plumes arising from an unstable background state and dissipating before reaching a fully nonlinear state, the above equations govern possibly stable plumes surrounded by core fluid that is otherwise convectively stable.

In the absence of any instability, steady source of buoyancy at the ICB would produce a plume of indefinite length. However, it is likely that any such plume is unstable (e.g., see Eltayeb and Loper, 1997; Classen et al., 1999; Eltayeb et al., 2005), leading to the production of a sequence of plumes governed by the equations presented above. It is not known at the present time whether such plumes are stable structures or are prone to further instability, but the scaling presented in the following section suggests that they are unstable.

8.06.5   Dynamics of the Plume Region

This section considers the dynamics of an ensemble of plumes within the plume region near the base of the outer core. This region is characterized by narrow, relatively isolated (having area fraction $f \ll 1$) regions of rapid upwelling (plumes) embedded in a broad region of downward flow. Due to the secular evolution of composition and entropy in the outer core, the descending fluid is stably stratified. Thus the structure of the plume region is similar to that encountered in the box-filling mode (Turner, 1975). The magnitudes and fluxes within the buoyant plumes are quantified in Section 8.06.5.1 and the dynamic stratification of the downwelling regions is quantified in Section 8.06.5.2.

8.06.5.1 Plume Flux

Dynamics of plumes may be cast in terms of the buoyancy flux, $\mathcal{J}$:

$$\mathcal{J} = C_0 g \dot{V}_p \qquad [42]$$

where total upward volume flux of plume material is

$$\dot{V}_p \sim 4\pi r^2 U_p f = A_p U_p n \qquad [43]$$

In this expression, n is the number of plumes which occupy an area fraction f of a spherical surface a distance r from Earth's center,

$$U_p = C_0 g \Lambda / 2\Omega \qquad [44]$$

and A_p is the horizontal area of a single plume:

$$A_p \sim \frac{L^2 \Lambda}{\cos(\theta)} \qquad [45]$$

Note that $U_p = \Lambda U$, with U given by [18] with $\bar{g}$ replaced by g, and $U_p = 2\Omega L$ with L given by [30].

If a steady plume were to rise through fluid that is neutrally buoyant, its buoyancy flux would be constant, independent of height, in spite of entrainment of ambient fluid.

Equations [42]–[45], together with [30], may be combined to yield expressions for C_0, U_p, and L in terms of $\mathcal{J}$ and other factors. The most uncertain of the other factors are f and n. Since these are related to $\mathcal{J}$ by

$$n \Lambda^2 \mathcal{J} = 128 \pi^2 r^4 \Omega^3 \overline{\cos(\theta) f^2} \qquad [46]$$

where an overbar denotes an average, the expressions for C_0, U_p, and L may take a number of forms. For example, elimination of n yields

$$C_0 \sim \sqrt{\frac{1}{2\Lambda f}} \left[\frac{1}{rg} \sqrt{\frac{\Omega \mathcal{J}}{\pi}} \right] \sqrt{\frac{1}{2\Lambda f}} C_* \qquad [47]$$

$$U_p \sim \sqrt{\frac{\Lambda}{2f}} \left[\frac{1}{2r} \sqrt{\frac{\mathcal{J}}{\pi \Omega}} \right] \sqrt{\frac{\Lambda}{2f}} U_* \qquad [48]$$

and

$$L \sim \sqrt{\frac{\Lambda}{2f}} \left[\frac{1}{4\Omega r} \sqrt{\frac{\mathcal{J}}{\pi \Omega}} \right] \sqrt{\frac{\Lambda}{2f}} L_* \qquad [49]$$

Alternately, elimination of f (setting $\overline{\cos(\theta)} = 1/2$) yields

$$C_0 \sim \frac{2\Omega}{g\Lambda} \left[\frac{\Omega \mathcal{J}}{n} \right]^{1/4} \qquad [50]$$

$$U_p \sim \left[\frac{\Omega \mathcal{J}}{n} \right]^{1/4} \qquad [51]$$

and

$$L \sim \frac{1}{2\Omega} \left[\frac{\Omega \mathcal{J}}{n} \right]^{1/4} \qquad [52]$$

Although the factors f and n are poorly known and quite variable, they do have firm limits: $f \leq 1$ and $n \geq 1$. A slightly more stringent limit applies to f, on the assumption that in the well-mixed region upwelling and downwelling plumes occupy similar areas, $f \leq 1/2$. These imply the following limits:

$$\frac{16 \pi^2 r^4 \Omega^3}{\mathcal{J} \Lambda^2} \geq n \geq 1 \qquad [53]$$

$$\frac{1}{2} \geq f \geq \frac{\Lambda}{16 \pi r^2 \Omega} \sqrt{\frac{\mathcal{J}}{\Omega}} \qquad [54]$$

$$\frac{1}{rg} \sqrt{\frac{\Omega \mathcal{J}}{\pi \Lambda}} \leq C_0 \leq \frac{2\Omega^{5/4} \mathcal{J}^{1/4}}{g\Lambda} \qquad [55]$$

$$\frac{1}{2r} \sqrt{\frac{\mathcal{J} \Lambda}{\pi \Omega}} \leq U_p \leq (\Omega \mathcal{J})^{1/4} \qquad [56]$$

and

$$\frac{1}{4\Omega r} \sqrt{\frac{\mathcal{J} \Lambda}{\pi \Omega}} \leq L \leq \frac{\mathcal{J}^{1/4}}{2\Omega^{3/4}} \qquad [57]$$

These scaling expressions are local (not involving radial derivatives) and thus are valid for plumes rising through surroundings that are not neutrally buoyant. However, $\mathcal{J}$ is not independent of radius (i.e., distance from the center of Earth) in that case.

In estimates [53]–[57], the left-hand limits apply to the well-mixed region (with $f = 1/2$), with right-hand limits possibly approached in the plume region, where $f \ll 1$. A plausible range of values for the buoyancy flux at the base of the outer core is $\mathcal{J}_{icb} \sim 15 \to 125 \, \text{m}^4 \, \text{s}^{-3}$ (see [94] and discussion following). For purposes of illustration, consider $\mathcal{J} \approx 50 \, \text{m}^4 \, \text{s}^{-3}$. An estimate for Λ comes from dynamo modeling; a plausible range of the typical magnetic field obtained by numerical simulations (Glatzmaier, personal communication, 2006) is between 0.01 and 0.05 Wb m^{-2}, giving a plausible range $25 < \Lambda < 626$. For purpose of illustration let $B_0 = 0.03$ Wb m^{-2}, which yields $\Lambda = 225$. Near the base of the outer core, $r = 1.3 \times 10^6$ m and $g = 4.5 \, \text{m s}^{-2}$, while in the interior, the mean values are appropriate: $\bar{r} = 2.76 \times 10^6$ m and $\bar{g} = 8.56 \, \text{m s}^{-2}$. With these numerical values, [53]–[57] become

$$7 \times 10^7 \geq n \geq 1 \qquad [58]$$

$$0.5 \geq f \geq 3 \times 10^{-5} \tag{59}$$

$$9.6 \times 10^{-11} \leq C_0 \leq 3.5 \times 10^{-8} \tag{60}$$

$$1.3 \times 10^{-3}\,\mathrm{m\,s^{-1}} \leq U_\mathrm{p} \leq 0.25\,\mathrm{m\,s^{-1}} \tag{61}$$

and

$$8.7\mathrm{m} \leq L \leq 1700\,\mathrm{m} \tag{62}$$

It is likely that $\mathcal{J}$ becomes small near the top of the outer core, in which case the above numerical estimates need to be modified appropriately. Further, the plume scaling does not apply within a stable region near the top of the outer core (if such a region exists). In particular, note that the velocity limits in [61] cannot be directly compared with the velocity estimated from secular variation because the value of $\mathcal{J}$ employed above is not representative of conditions near the top of the outer core.

Within the plume region near the base of the outer core, the fact that number of plumes is proportional to the square of f suggests two things. First, within the plume region, plumes are few in number, large, and vigorous. Second, as the plumes rise, they become more numerous, smaller, and weaker. This implies that the plumes are unstable, breaking up as they rise.

8.06.5.2 Relative Magnitudes of Forces and Fluxes

With these scalings, the relative magnitude of the viscous force is quantified by the Ekman number, written as

$$E = \frac{16\pi r^2 \Omega^2 \nu}{\mathcal{J}} f \sim 0.02 f \tag{63}$$

and the magnitude of the perturbation magnetic field produced by an individual plume, relative to the applied field, is

$$\frac{R_\mathrm{m}}{\Lambda} = \frac{\mathcal{J}}{16\pi r^2 \Omega^2 \eta_\mathrm{m} f} \sim \frac{1.2 \times 10^{-5}}{f} \tag{64}$$

The numerical estimates are suitable for the middle of the outer core. The appearance of the factor Λ in the denominator on the left-hand side of [64] is due to the fact that for plumes the relative magnitude of advection relative to diffusion is given by

$$\frac{(\mathbf{u}\cdot\nabla)}{\nabla^2} \sim \frac{2\Omega L^2}{\Lambda} \sim \frac{2.4 \times 10^{-5}}{f} \tag{65}$$

It follows that the Schmidt and Prandtl numbers for plume flow are

$$S_\mathrm{ch} = \frac{\mathcal{J}}{16\pi r^2 \Omega^2 Df} \sim \frac{3400}{f} \tag{66}$$

and

$$P_\mathrm{r} = \frac{\mathcal{J}}{16\pi r^2 \Omega^2 \bar{\kappa} f} \sim \frac{8}{f} \tag{67}$$

The numerical estimates in [63], [64], [66], and [67] employ the molecular values of viscosity and magnetic diffusivity; see the table of notation. It is clear that molecular viscosity, thermal diffusion, and material diffusion are small for all possible values of f, while magnetic induction in a single plume may become appreciable if $f \leq 1.2 \times 10^{-5}$. (Recall that the equations presented in Section 8.06.4 are valid only if magnetic induction is negligible.)

8.06.5.3 Plume Dynamo Action

It is not known whether individual small-scale buoyant plumes contribute positively to dynamo action. Assuming that they do, the combined and cumulative effect of an ensemble of small-scale buoyant plumes on the dynamo process is unknown, but it has the potential to be important. In fact, it was found in Section 8.06.5.2 that the effective magnetic Reynolds number of individual plumes may be of unit order provided $f \leq 1.2 \times 10^{-5}$. If the dynamo action of individual plumes were additive, the total effect would be quantified by $n_\mathrm{B} R_\mathrm{m}/\Lambda$, where n_B is the number of plumes threaded by a given line of force. Given that the lateral extent of individual plumes is of order L and assuming that they occupy a fraction f of a given line of force having length h, it follows that $n_\mathrm{B} = fh/L$. Using this, [49] and [64] give

$$n_\mathrm{B}\frac{R_\mathrm{m}}{\Lambda} = \left[\frac{h}{4\pi\Omega\eta_\mathrm{m}}\right]\sqrt{\frac{2\pi f\mathcal{J}}{\Omega\Lambda}} \tag{68}$$

With previous numerical estimates, this equation predicts the potential for significant dynamo action if $h\sqrt{f} > 8 \times 10^5$ m. Again it should be emphasized that these quantitative estimates, and the assumption of additive dynamo effect, are very uncertain. However, since $f \leq 1$ by definition, it appears that plumes can provide significant dynamo action only if the extent of a given line of force is larger than the depth of the core. This can be the case; in the

strong-field limit, the field is dominated by a strong toroidal field which is predominantly aligned in the zonal direction.

8.06.5.4 Stratification in Downwelling Regions

Due to the secular evolution of the outer core, successive layers of fluid descending toward the ICB are progressively more buoyant, making the core in such regions stably stratified. The structure of plumes near the bottom of the outer core is likely to be affected by this stratification, which is quantified in this subsection.

Local stratification is typically quantified by the Brunt–Väisälä frequency of the form

$$N \simeq \sqrt{g \mid dC/dr \mid} \qquad [69]$$

Near the base of the outer core, $g \approx g_{icb}$, while the vertical gradient of co-density, using [10], is

$$\frac{dC}{dr} = -\alpha_s \frac{ds_c}{dr} - \frac{dc_c}{dr} \qquad [70]$$

(The derivative of α_s is assumed small.) At the ICB, $\alpha_s \approx 6.5 \times 10^{-5}$ K kg J^{-1}.

Assuming that the descending motion is locally steady and vertical and writing $\mathbf{u} = -W\hat{\mathbf{r}}$, where $\hat{\mathbf{r}}$ is a unit vector pointing upward and using [11] (with $F_c = 0$) and [12] (with $F_s = 0$), [70] becomes

$$dC/dr = \dot{C}/W \qquad [71]$$

where

$$\dot{C} \equiv \alpha_s \dot{s}_* - \alpha_s \dot{s}_a - \dot{c}_a = [1.7x_{rd} + 1.7x_{oh} - 11.5] \times 10^{-20} \text{s}^{-1}$$
$$[72]$$

and the numerical estimates following [14] have been used. It is unlikely that the rate of heating due to radioactivity or Ohmic dissipation is sufficiently large to make this gradient positive. Assuming, for example, that $x_{rd} + x_{oh} \approx 3$ (i.e., the rate of internal heating due to radioactive decay and Ohmic heating is 3×10^{12} W), $\dot{C} \approx 5 \times 10^{-20}\text{s}^{-1}$. By conservation of volume, in the limit that $f \ll 1$, the speed of downwelling is given by

$$W = 2\Omega L f \sim \sqrt{2f\Lambda} \left[\frac{1}{4r} \sqrt{\frac{\mathcal{J}}{\pi\Omega}} \right]$$
$$\sim \sqrt{2f\Lambda} \, 4 \times 10^{-5} \text{m s}^{-1} \qquad [73]$$

where [48] has been used. Using $\Lambda = 225$, $W \sim \sqrt{2f}$ 6×10^{-4}m s^{-1}. Combining [71] and [73] gives

$$\frac{dC}{dr} \sim \frac{1}{\sqrt{2f\Lambda}} \left[4r\dot{C}\sqrt{\frac{\pi\Omega}{\mathcal{J}}} \right] \qquad [74]$$

and, recalling that dC/dr and $\dot{C}$ are negative, the Brunt–Väisälä frequency due to compositional stratification is

$$N = \sqrt{g\left|\frac{dC}{dr}\right|} \sim \sqrt{4rg|\dot{C}|\sqrt{\frac{\pi\Omega}{\mathcal{J}2f\Lambda}}} \sim \frac{10^{-7}}{(f\Lambda)^{1/4}} \text{ s}^{-1} \quad [75]$$

This translates to an oscillation period of $(f \Lambda)^{1/4}$ 0.32 years or, if $\Lambda = 225$, $f^{1/4}$ 0.25 years. Further, if f were to achieve the smallest value quoted in the paragraph following [54], the period of oscillation would be about 5 days. While the magnitudes of these estimates are somewhat uncertain, they demonstrate that a significant degree of stratification is theoretically possible, and that strength of stratification increases as f decreases; that is, the stratification of descending material becomes progressively stronger as it approaches the ICB.

8.06.6 Cascades and Transfers of Energy in Core Turbulence

Perhaps the greatest difference between classic turbulence and turbulence in Earth's core is in the cascade of energy. In classic turbulence, kinetic energy is fed in at large scales and it cascades through the so-called inertial range to smaller scales, until viscous dissipation transforms it to heat. In contrast, in the core, the cascade process involves the Lorentz force which is dissipative at all scales. That is, there is nothing like an inertial range in which energy is transferred without loss. In particular, Siso-Nadal and Davidson (2004) have shown that the structure of a vortex in a homogeneous rotating hydromagnetic fluid evolves rapidly (on a scale of days) to a shape that minimizes the effects of the Coriolis and Lorentz forces. It is very likely that flows driven by buoyancy will have this same general characteristic of minimizing these forces. A likely shape is one flattened in the plane of $\mathbf{\Omega}$ and $\mathbf{B}$; this is the pancake shape identified by Braginsky and Meytlis (1990; see Section 8.06.4).

The existence of the inertial range also relies on an input of kinetic energy at the largest scales of motion, often by mechanical means, such as forced convection. If instead the energy of fluid motion is

supplied by buoyancy forces (as is the case for most geophysical flows), the situation may be quite different. In order to generate large-scale structures, there must be a significant and reasonably efficient cascade of energy up the spatial scale. This is known to occur in the atmosphere and oceans due to the constraint imposed by the Coriolis force, coupled with the extreme aspect ratio of the fluid bodies (having depth much smaller than lateral extent; e.g., see Starr, 1968). It is not clear whether a similar process will act in the outer core, which is subject to the action of the Lorentz force and which is a deep fluid.

Given that the dynamo has a limited energy supply (*see* Chapter 8.02), it is apparent that the dynamo must avoid flows and structures that dissipate energy strongly on small scales. One way to accomplish this is to have the energy fed in at the largest dynamically possible scale, with virtually no cascade of energy to smaller scales. Another is to have the small-scale flow structures configured in a way to minimize Ohmic dissipation. At this point, our knowledge of the dynamics of small-scale flow structures is inadequate to determine which, if either, alternative is preferred.

8.06.7   Approaches to Parametrization of Turbulence

Numerical simulations of convection and dynamo action applicable to Earth's core are forced to operate in regions of parameter space far removed from core conditions. There are two reasons for this: limitations of speed and storage in current computers and the need for numerical stability. A good review of these limitations is given by Glatzmaier (2002). The first of these limitations will be with us for a very long time, while the second can be remedied by the advent of better numerical schemes.

Given the wide disparity in scales between the observed magnetic field ($\sim 10^6$ m) and dissipation of kinetic energy by molecular viscosity (<1 m), it is clear that some sort of parametrization of the smaller scales is necessary in numerical simulations of core dynamics and the dynamo process. Less clear are the processes to be parametrized and the proper form of the parametrizations. For example, scalar dissipative parametrizations are poor approximations to nonisotropic and nondiffusive processes.

8.06.7.1   The Need for Parametrization

The full set of governing equations consist of four evolution equations plus a diagnostic equation to be solved for two vectors (velocity and magnetic field) and three scalars (pressure, composition, and entropy). The molecular form of these equations contain four diffusivities: η_m, ν, κ, and D. However, the relatively large value of magnetic diffusivity permits the Lorentz force and the equation for the magnetic field to be linearized for small-scale flows, effectively obviating the need for parametrization. That leaves fluxes of momentum, material, and heat to be parametrized.

Consider first the momentum equation, [24], and the need to parametrize viscous momentum flux. The magnitude of molecular viscosity is very small, so that parametrization appears inevitable. However, it first must be determined whether parametrization is necessary. With current numerical models, parametrization of the viscous force is necessary to achieve numerical stability. However, there are numerical schemes on the horizon (such as WENO; see Jiang and Wu, 1999) that are numerically convergent with very small viscosity. Once such schemes are adopted, this requirement will disappear.

The question to be addressed now is whether, and under what circumstances, the viscous force is important and must be parametrized in numerical simulations. Viscosity is well known to be important in thin layers, such as the Ekman and Stewartson layers. Current numerical simulations explicitly resolve the Ekman layer, and this imposes a significant constraint on the choice of grid spacing and magnitude of viscosity. This limitation could be removed by the use of Ekman–Hartmann compatibility conditions; see Loper (1970). Further, when hydromagnetic effects are present, they dominate the Stewartson-layer structure, making the viscous force irrelevant; see Hollerbach (1996). In sum, there appears to be no need to parametrize small-scale viscous structures such as boundary layers.

What is rather less well known is the role of the viscous force in determining large-scale structure in flows driven by buoyancy forces, as is the case in Earth's core. Shimizu and Loper (1997) showed that, no matter how small the molecular viscosity, the viscous force is important in determining the scale of rotating hydromagnetic flow structures driven by buoyancy. This importance may be understood by realizing that both the Coriolis and Lorentz forces are anisotropic and provide no constraint on the shearing structure of flows that lie in the plane of $\boldsymbol{\Omega}$ and $\mathbf{B}$; the viscous force must provide that constraint. The extent of the flow structures which involve viscosity is quite large, and may not be realized in the outer core, which is of finite size.

The parametrized form of turbulent diffusion of entropy and material should mirror the structure of the relevant fluid motions. That is, the effective diffusivities should be anisotropic, having a structure such as that proposed by Braginsky and Meytlis (1990), as described in the following subsection.

8.06.7.2   Diffusive Parametrizations

The simplest form of parametrization is that dictated by molecular processes, using greatly enhanced coefficients, often called eddy diffusivities. "All models of the geodynamo crudely approximate . . . turbulent transport as a simple, isotropic, homogeneous, diffusive process modeled after molecular diffusion but with an enhanced 'turbulent diffusivity'." (Glatzmaier, 2002). This approach has been surprisingly successful, producing earth-like dynamos in numerical simulations. However, these simulated dynamos require a large amount of power – more than the Earth is likely to be able to supply. The diffusive coefficients used in current 3-D numerical simulations are sufficiently large that the resolved scales of motion are stable and the flow fields are in fact laminar. Glatzmaier (2005) has noted that turbulent motions are likely to be significantly different than laminar, so it is important to reduce the diffusivities and run 3-D models in the turbulent regime.

A variant on the eddy diffusivity approach is to use hyperdiffusivities, in which the magnitude of the diffusion coefficient increases as the lengthscale decreases. This has the advantage of reducing the amount of dissipation at larger scales, while providing numerical stability. The utility of this approach has been summarized by Glatzmaier (2002).

The influence of Coriolis and Lorentz forces is nonisotropic and a better parametrization will correspondingly entail nonisotropic (tensorial) eddy diffusivities. A heuristic model has been proposed by Braginsky and Meytlis (1990; summarized in appendix C of Braginsky and Roberts, 1995). In this model, the scalar viscosity is replaced by a tensor with principal axes locally aligned with $\mathbf{\Omega}$ and $\mathbf{B}$ such that the in-plane viscosity is of the same magnitude as magnetic diffusion (i.e., on the order of $1 \, \mathrm{m^2 \, s^{-1}}$), while that normal to the plane is smaller by a factor 10^{-3}. The parametrizations of diffusion of heat and material are the same as for viscosity.

8.06.7.3   Alternative Parametrizations

A fundamental shortcoming of all diffusive parametrizations is their inability to simulating non-diffusive processes that alter the scale and structure of flow and field. As a result, diffusive parametrizations tend to overpredict dissipation of magnetic and kinetic energy and misrepresent the dynamical structures. Several approaches have been suggested to circumvent this limitation, including the similarity and alpha models. Common features of these models are a smoothing operation and a closure assumption.

The similarity model is based on a premise and an assumption. The premise is that the dominant sub-grid scales are those just below the resolution of the large-eddy simulation (LES) at hand. The assumption is that the structure of largest unresolved scales is similar to that of the smallest resolved scales. The development of the similar model entails the application of a series of smoothing operations of the form

$$\bar{\mathbf{u}}(\mathbf{r}, \, t) = \int G(\mathbf{r} - \mathbf{r}') \mathbf{u}(\mathbf{r}', \, t) \mathrm{d}\mathbf{r}' \qquad [76]$$

where the smoothing operator, G, is typically Gaussian in form. Closure is achieved by assuming that the fluctuations to be parametrized are similar in form to those of the smallest resolved scales. Initial implementation of this method appeared promising; it clearly outperforms eddy-diffusive models (Buffett, 2003). However, recent results indicate that this method is of limited utility; its ability to accurately predict the structure of the subgrid processes seems to decrease fairly rapidly with scale separation.

The alpha model employs smoothing of small-scale fluctuations on a Lagrangian trajectory, with the result expressed in the usual Eulerian framework. The smoothing process can be cast in the form of [76]. The parameter alpha, which gives the method its name, is a lengthscale separating large-scale, active motions from small-scale passive motions. The formulation is closed, for example, by using Taylor's hypothesis of 'frozen-in' turbulence. For details, see Holm (2002). Like the similarity model, the alpha model is much in its infancy and it has yet to be demonstrated that it is capable of resolving small-scale structures accurately.

8.06.8   Unresolved Issues and Future Directions

The goal of numerical simulations of core dynamics and the geodynamo is to operate in parameter

regimes where the results are relevant to Earth's core. Initial results with crude parametrizations, involving large eddy diffusivities, have been very promising, but these results are for parameters far from 'Earth like'. In order to make progress, a combination of advances needs to be made, including the use of larger and faster machines, the use of better algorithms (such as WENO, that do not need dissipation for numerical stability), and the use of better parametrizations of small-scale structures near boundaries (such as the Ekman or Ekman–Hartmann layer) and in the interior of the core (associated with turbulence and energy cascades).

Bigger and faster machines will be developed at a fairly predictable pace, but given the disparity between currently resolved scales and the smallest dynamic scales in the core, there is little hope of solving the geodynamo completely by direct numerical simulation (i.e., by brute force). Major advances can be made fairly quickly and economically by adopting new numerical schemes that do not need large dissipations for numerical stability, and parametrizations that obviate the need to resolve viscous boundary layers. However, the problem of parametrizing the unresolved scales will remain for some time to come.

Regarding turbulence and energy cascades, relatively little is known of 'mesoscale' dynamics, on scales having small magnetic Reynolds, Ekman, Peclet, and Schmidt numbers. Key questions that remain to be resolved include:

- On what scale is energy fed into convective motions by buoyancy forces?
- Is there a significant cascade of mechanical energy to larger spatial scales?
- With a linearized momentum equation, how does the energy cascade occur?
- On what scales is mechanical energy degraded to heat?
- Are there configurations of flow and field for which energy losses during cascade are small?
- Does the core adopt these loss-minimization structures?
- What is the energy requirement of the geodynamo?
- Is viscosity important in determining core flow structures or energy dissipation?

Once answers to these questions have been obtained, then dynamically consistent parametrizations may be devised and implemented.

Appendix 1: Core Evolution and Buoyancy Flux

This appendix contains essential background material for the main body of the chapter quantifying the evolution of the composition and entropy in the outer core. First the secular evolution of composition and specific entropy in the outer core are quantified. Sources of specific entropy are quantified next. Finally, the sources are combined to quantify the buoyancy flux.

Evolution of Composition

It follows from conservation of the heavy and light constituents of the core that the rate of evolution of the composition of the outer core is given by

$$\dot{c}_a = \delta \dot{M}_{ic}/M_{oc} \qquad [77]$$

where δ is the fractional jump in density due to change of composition across the ICB, M_{oc} is the mass of the outer core, and $\dot{M}_{ic} = dM_{ic}/dt$ is the rate of growth of the solid inner core. A reasonable estimate based on eigenfrequencies of normal modes of Earth oscillation, is $\delta \approx 0.05$ (Masters and Gubbins, 2003). The magnitude of $\dot{M}_{ic}$ is uncertain and somewhat controversial, but there is little doubt that the inner core is growing, and that $\dot{c}_a > 0$. The estimate $\dot{c}_a \approx 9 \times 10^{-20}$ s^{-1} by Roberts and Glatzmaier (2000) corresponds to a growth rate $\dot{M}_{ic} = 3.5 \times 10^6$ kg s^{-1}; if the inner core grew at this constant rate, its age would be 0.9 Ga.

The secular change of the reference-state composition acts as a volumetric sink of buoyant material within the outer core in eqn [11] governing the convective perturbation, c_c. A counterbalancing source is provided at the ICB by the solidification process. A fluid parcel gains light material as it passes close to the ICB (or as it penetrates the uppermost layers of the mushy inner core), with the change given by

$$(\Delta c_c)_{icb} = \delta \dot{M}_{ic}/(\dot{M})_{icb} = \dot{c}_a \tau_{oc} \qquad [78]$$

where $\dot{M}$ is the convective mass flux (being a function of radius), $(\dot{M})_{icb}$ is that flux evaluated at the ICB, and $\tau_{oc} = M_{oc}/(\dot{M})_{icb}$ is the mean turnover time of the outer core.

Written in terms of the buoyancy flux, [78] is

$$(\mathcal{F}_c)_{icb} = \delta [g/\rho]_{icb} \dot{M}_{ic} \approx \delta g_{icb} \dot{V}_{ic} \qquad [79]$$

where $\mathcal{F}_c = c_c g \dot{V}$ is the buoyancy flux due to composition, $\dot{V}_{ic} = \dot{M}_{ic}/\bar{\rho}_{ic}$ is the rate of growth of the volume of the inner core, and $\bar{\rho}_{ic}(\approx \rho_{icb})$ is the mean density of the inner core. The rate of growth

of the inner core is somewhat uncertain; one way to parametrize it is to write $\dot{V}_{ic} = V_{ic}/\tau_{ic}$, where V_{ic} ($= 7.6 \times 10^{18}\,m^3$) is the current volume of the inner core and τ_{ic} would be the age of the inner core if its volume had increased at a constant rate. Estimates of τ_{ic} vary from about 0.5 to 4.0 Ga ($\tau_{ic} \approx 1.6 \rightarrow 13 \times 10^{16}\,s$), giving $(\mathcal{J}_c)_{icb} \approx 13 \rightarrow 105\,m^4\,s^{-3}$. This is a relatively modest buoyancy flux; black smokers and other sources of buoyancy in the ocean typically have far greater magnitudes.

Assuming that there are no significant sources or sinks of material at the CMB, the variation of this buoyancy flux with radius in the outer core is given by

$$\mathcal{J}_c = (\mathcal{J}_c)_{icb}[M_c - M]/M_{oc} \qquad [80]$$

where $M(r)$ is the mass within a sphere of radius r and M_c ($\sim 1.94 \times 10^{24}/kg$) is the mass of the core. The buoyancy flux is related to the power, P_c, released by the rearrangement of matter in the outer core:

$$P_c = \int_{r_{icb}}^{r_{cmb}} \mathcal{J}_c \rho\, dr \qquad [81]$$

Using data in Stacey and Davis (2004), plus the estimated range of τ_{ic} given above, $P_c \approx 0.24 \rightarrow 1.9 \times 10^{12}$ W. This power is sufficient to drive the dynamo in the strong-field regime (Roberts *et al.* (2003) and *see* Chapter 8.02), even in the absence of a contribution from the specific entropy. However, if most of this energy is dissipated by small-scale motions, the amount available to sustain the large-scale field will be correspondingly smaller.

Evolution of Specific Entropy

The specific entropy of the outer core decreases with time due to the progressive cooling (Gubbins *et al.*, 2003):

$$\dot{s}_a \approx -Q_{sc}/\bar{T}M_c \qquad [82]$$

where

$$\bar{T} = \frac{1}{M}\int_{core} T\rho\, dV \qquad [83]$$

is the mean temperature of the core ($\bar{T} \approx 4350\,K$) and Q_{sc} is the heat flux from core to mantle resulting from secular cooling of the core. The other source of heat from radioactive decay is, in effect, of external origin and so does not contribute to the secular entropy change. The contribution to [82] due to the rearrangement of material associated with the growth of the inner core is negligibly small.

In addition to the sensible cooling of the core, secular cooling includes the latent heat and gravitational energy released by the growth of the inner core; altogether

$$Q_{sc} = C_{pe}M_c[-d\bar{T}/dt] \qquad [84]$$

where $C_{pe} = \bar{C}_p + C_{gr} + C_{lh}$ is the effective specific heat of the core, $\bar{C}_p$ ($\approx 800\,J\,kg^{-1}\,K^{-1}$) is the mean (mass averaged) specific heat, and the effective specific heats for gravitational energy and latent heat are given by

$$C_{gr} = \left[\frac{M_{ic}}{\Gamma M_{oc}}\right]\frac{[\Delta\rho]\bar{\psi}}{\rho\bar{T}} \approx 300\,\frac{J}{kg\ K} \qquad [85]$$

and

$$C_{lh} = \left[\frac{M_{ic}}{\Gamma M_c}\right]\frac{L}{\bar{T}} \approx 600\,\frac{J}{kg\ K} \qquad [86]$$

where M_{ic} ($\approx 9.84 \times 10^{22}\,kg$) and M_{oc} ($\approx 1.84 \times 10^{24}$ kg) are the masses of the inner and outer cores, $M_c = M_{oc} + M_{ic}$, $\bar{\psi}$ ($\approx 10^7\,J\,kg^{-1}$) is the mean gravitational potential of the outer core, and

$$\Gamma = \left[\frac{\alpha\rho_a g_a r}{3\rho_a C_p + 6K_S\alpha^2 T}\right]_{icb} \qquad [87]$$

is a measure of the rate of advance (increase of radius with time) of the intersection of the adiabat with the melting curve as the core cools; K_S is the adiabatic incompressibility. With previous estimates, $\Gamma \approx 0.02$.

Note that with these estimates, a relatively modest rate of cooling of, say, $1.14 \times 10^{-15}\,K\,s^{-1}$ ($= 36\,K\,Ga^{-1}$) releases heat at a rate sufficient to equal that conducted down the adiabat at the CMB (3.6×10^{12} W with $k = 28\,W\,m^{-1}\,K^{-1}$). Note that $C_{pe}M_c \approx 10^{11}$ W Ga K^{-1}, so that a change of cooling rate of $10\,K\,Ga^{-1}$ corresponds to a change of heat flux of 10^{12} W. For purposes of illustration, suppose that 5×10^{12} W are released by cooling of the core, corresponding to a cooling rate of $50\,K\,Ga^{-1}$. With a convective turnover time of 3700 years, the core cools by about $\Delta T = 2 \times 10^{-4}$ K each convective cycle.

The cooling rate of the core is somewhat uncertain. This may be quantified by writing $d\bar{T}/dt = -x_\Gamma$ $10\,K\,Ga^{-1} \approx -x_\Gamma\ 3 \times 10^{-16}\,K\,s^{-1}$, so that a value $x_\Gamma = 1$ corresponds roughly to 10^{12} W of core cooling. Altogether, $\dot{s}_a \approx -1.2x_\Gamma \times 10^{-16}\,W\,kg^{-1}\,K^{-1}$. The value ($\dot{s}_a \approx -3.7 \times 10^{-16}\,W\,kg^{-1}\,K^{-1}$) estimated by Roberts and Glatzmaier (2000) is achieved if the rate of heat loss from the core is 3.4×10^{12} W.

Specific-Entropy Sources

The variation of specific entropy within the outer core is more complicated than that of composition, for two reasons. First, [12] contains source terms other than that due to secular evolution of the reference state, and second, the specific entropy is changed due to exchanges of heat at the CMB as well as at the ICB. In this subappendix, first the three volumetric entropy sources that contribute to $\dot{s}_*$ (see [13]) are estimated close to the ICB, then the boundary sources at the ICB and CMB are estimated.

Volumetric sources

It is reasonable to assume that Ohmic heating is uniformly distributed (by mass) in the entire core so that

$$q_{oh} = Q_{oh}/M_c \qquad [88]$$

It is likely, due to segregation induced by the solidification process, that radioactive heating is concentrated in the outer core, so that

$$q_{rd} = Q_{rd}/M_{oc} \qquad [89]$$

There is substantial uncertainty in each of the three volumetric sources. It is uncertain whether there is a significant amount of radioactive heating in the core. The efficiency of the dynamo mechanism and the associated amount of Ohmic heating is not well constrained. While the radial structure of the adiabat is well constrained, the value of thermal conductivity is controversial. The uncertainties in heat sources will be accommodated by writing $Q_{rd} = x_{rd}\, 10^{12}$ W and $Q_{oh} = x_{oh}\, 10^{12}$ W. The value of thermal conductivity will be taken as $k = 28$ W m^{-1} K^{-1} (F. Stacey, personal communication, 2005), with $\nabla^2 T_a \approx -7 \times 10^{-10}$ K m^{-2}. Altogether, near the ICB, $\{q_{rd},\ q_{oh},\ k[\nabla^2 T_a]/\rho_a\} = \{5.4x_{rd},\ 5.2x_{oh},\ -15\} \times 10^{-13}$ W kg^{-1} and with $T_{icb} \approx 5000$ K $\dot{s}_* = [2.7x_{rd} + 2.6x_{oh} - 7.5] \times 10^{-16}$ W kg^{-1} K^{-1}.

Boundary sources

At the ICB, latent heat and inner-core sources increase s_c, while at the CMB, heat loss to the mantle (over and above that carried by conduction) decreases s_c. These changes are quantified by

$$(\Delta s_c)_{icb} = [Q_{lh} + Q_{ic}]/(MT_a)_{icb} \qquad [90]$$

and

$$(\Delta s_c)_{cmb} = [Q_{cd} - Q]/(\dot{M}T_a)_{cmb} \qquad [91]$$

where

$$Q_{lh} = L_H \dot{M}_{ic} \qquad [92]$$

is the rate of latent heat release due to solidification, Q_{cd} is the rate of transfer of heat by conduction down the adiabat, Q is the total rate of heat transfer from core to mantle, and L_H is the latent heat of fusion. The rate, Q_{ic}, of heat transfer from the inner core is due to those fractions of core secular cooling, Q_{sc}, and Ohmic dissipation, Q_{oh}, that occur within the inner core (with radioactive heating in the inner core being assumed small). The former is proportional to the potential temperature, giving

$$Q_{ic} = \frac{M_{ic}}{M_c}\left[\frac{\bar{T}_{ic}}{\bar{T}_c} Q_{sc} + Q_{oh}\right] = 0.057Q_{sc} + 0.05Q_{oh} \qquad [93]$$

In a rough calculation, the effect of Q_{ic} may be ignored.

Buoyancy Flux

The changes of both composition and specific entropy at the ICB make the rising fluid buoyant and drive vigorous convection near the base of the outer core. Without loss of generality, the co-density of the descending fluid at the base of the outer core may be set equal to zero. The co-density of the fluid rising from the ICB is related to the buoyancy flux, $\mathcal{J}$, at the base of the outer core by

$$\mathcal{J}_{icb} = \left[Cg\dot{V}\right]_{icb} = -\left[L_H(\alpha/C_p)_{icb} + \delta\right]g_{cb}\dot{V}_{ic} \qquad [94]$$

Using data from Gubbins *et al.* (2003) and Stacey and Davis (2004), $L_H\ (\alpha/C_p)_{icb} \approx 0.01$. Recalling that $\delta \approx 0.05$, it appears that change of composition is several times more important that latent heat in creating buoyancy at the ICB. Using previous estimates of τ_{ic} and other parameters, $\mathcal{J}_{icb} \approx 15 \rightarrow 125$ m^4 s^{-3}.

Barring significant mass exchanges at the CMB, the buoyancy at the top of the mantle is dominated by the change of specific entropy. If $Q > Q_{cd}$, this change drives convection near the top of the outer core.

References

Braginsky SI (1999) Dynamics of the stably stratified ocean at the top of the core. *Physics of the Earth and Planetary Interiors* 111: 21–34.

Braginsky SI and Meytlis VP (1990) Local turbulence in the Earth's core. *Geophysical and Astrophysical Fluid Dynamics* 755: 71–87.

Braginsky SI and Roberts PH (1995) Equations governing convection in Earth's core and the geodynamo. *Geophysical and Astrophysical Fluid Dynamics* 79: 1–97.

Buffett BA (2003) A comparison of subgrid-scale models for large-eddy simulations of convection in the Earth's core. *Geophysical Journal International* 153: 753–765.

Cambon C (2001) Turbulence and vortex structures in rotating and stratified flows. *European Journal of Mechanics B* 20: 489–510.

Cambon C, Mansour NN, and Godeferd FS (1997) Energy transfer in rotation turbulence. *Journal of Fluid Mechanics* 337: 303–332.

Chalmers B (1964) *Principles of Solidification*. New York: Wiley.

Chandrasekhar S (1961) *Hydrodynamic and Hydromagnetic Stability*. Oxford: Clarendon Press.

Charney JG (1971) Geostrophic turbulence. *Journal of Atmospheric Science* 28: 1087–1095.

Classen S, Hempel M, and Christensen U (1999) Blob instability in rotating compositional convection. *Geophysical Research Letters* 26: 135–138.

Davidson PA (2000) *An Introduction to Magnetohydrodynamics*, 422pp. Cambridge: Cambridge University Press.

Eltayeb IA, Hamza EA, Jervase JA, Krishnan E, and Loper DE (2005) Compositional convection in the presence of a magnetic field. Part II. Cartesian plume. *Proceedings of the Royal Society of London* 461: 2605–2633.

Eltayeb IA and Loper DE (1997) On the stability of vertically oriented double diffusive interfaces. Part 3. Cylindrical interface. *Journal of Fluid Mechanics* 353: 45–66.

Glatzmaier GA (2002) Geodynamo simulations – How realistic are they? *Annual Review of the Earth and Planetary Science* 30: 237–257.

Glatzmaier GA (2005) Planetary and stellar dynamos: Challenges for next generation models. In: Soward AM, Jones CA, Hughes DW, and Weiss NO (eds.) *Fluid Dynamics and Dynamos in Astrophysics and Geophysics*, pp. 331–357. Boca Raton: CRC Press.

Gubbins D, Alfe D, Masters G, Price GD, and Gillan MJ (2003) Can the Earth's dynamo run on heat alone? *Geophysical Journal International* 155: 609–622.

Hollerbach R (1996) Magnetohydrodynamic shear layers in a rapidly rotating plane layer. *Geophysical and Astrophysical Fluid Dynamics* 82: 237–253.

Holm DD (2002) Lagrangian averages, averaged Lagrangians, and the mean effects of fluctuations in fluid dynamics. *Chaos* 12: 518–530.

Jiang G-S and Wu CC (1999) A high-order WENO finite difference scheme for ideal magneto-hydrodynamics. *Journal of Computational Physics* 150: 561–594.

Loper DE (1970) General solution for the linearized Ekman-Hartmann layer on a spherical boundary. *Physics of Fluids* 13: 2995–2998.

Loper DE and Roberts PH (1981) A study of conditions at the inner core boundary of the earth. *Physics of the Earth and Planetary Interiors* 24: 302–307.

Masters G and Gubbins D (2003) On the resolution of density within the Earth. *Physics of the Earth and Planetary Interiors* 140: 159–167.

Merrill RT, McElhinney MW, and McFadden PL (1996) *The Magnetic Field of the Earth: Paleomagnetism, the Core and the Deep Mantle*, 531pp. San Diego: Academic Press.

Moffatt HK (1967) On the suppression of turbulence by a uniform magnetic field. *Journal of Fluid Mechanics* 28: 571–592.

Moffatt HK (1978) *Magnetic Field Generation in Electrically Conducting Fluids*, 343pp. Cambridge: Cambridge University Press.

Pedlosky J (1987) *Geophysical Fluid Dynamics* 2nd edn., 710pp. New York: Springer.

Poirier JP (1988) Transport properties of liquid metals and viscosity of the Earth's core. *Geophysical Journal* 92: 99–105.

Rhines PB (1979) Geostrophic turbulence. *Annual Review of Fluid Mechanics* 11: 401–441.

Roberts PH and Glatzmaier GA (2000) Geodynamo theory and simulations. *Review of Modern Physics* 72: 1081–1123.

Roberts PH, Jones CA, and Calderwood AR (2003) Energy fluxes and Ohmic dissipation in the earth's core. In: Jones C, Soward A, and Zhang K (eds.) *Earth's Core and Lower Mantle*. London: Taylor and Francis.

Shimizu H and Loper DE (1997) Time and length scales of buoyancy-driven flow structures in a rotating hydromagnetic fluid. *Physics of the Earth and Planetary Interiors* 104: 307–329.

Siso-Nadal F and Davidson PA (2004) Anisotropic evolution of small isolated vortices within the core of the Earth. *Physics of Fluids* 16: 1242–1254.

Stacey FD and Anderson OL (2001) Electrical and thermal conductivities of Fe-Ni-Si alloy under core conditions. *Physics of the Earth and Planetary Interiors* 124: 153–162.

Stacey FD and Davis PM (2004) High pressure equations of state with applications to the lower mantle and core. *Physics of the Earth and Planetary Interiors* 142: 137–184.

Starr VP (1968) *Physics of Negative Viscosity Phenomena*, 255pp. New York: McGraw-Hill.

Turner JS (1975) *Buoyancy Effects in Fluids*. Cambridge: Cambridge University Press.